

# Entanglement entropy for nonzero genus topologies

S. Santhosh Kumar<sup>1,\*</sup>, Suman Ghosh<sup>2,†</sup> and S. Shankaranarayanan<sup>1,‡</sup>

<sup>1</sup>*School of Physics, Indian Institute of Science Education and Research(IISER-TVM), Thiruvananthapuram- 695 016, India and*

<sup>2</sup>*Department of Theoretical Sciences, S.N. Bose National Centre for Basic Sciences, Salt Lake, Kolkata- 700 098, India*

Over the last three decades entanglement entropy has been obtained for quantum fields propagating in Genus-0 topologies (spheres). For scalar fields propagating in these topologies, it has been shown that the entanglement entropy scales as area. In the last few years nontrivial topologies are increasingly relevant for different areas. For instance, in describing quantum phases, it has been realized that long-range entangled states are described by topological order. If quantum entanglement can plausibly provide explanation for these, it is then imperative to obtain entanglement entropy in these topologies. In this work, using two different methods, we explicitly show that the entanglement entropy scales as area of the Genus-1 geometry.

PACS numbers: 11.10-z, 03.65 ud, 04.50Gh, 04.70Dy

## I. INTRODUCTION

Black holes have posed many puzzles, such as the information paradox and origin of Bekenstein-Hawking entropy, which are related to fundamental principles of general relativity and quantum physics. Although there have been several proposals to understand these, none of these have provided any consistent framework [1] (For recent reviews, see Refs. [2–4]). Quantum entanglement is one approach that naturally provide physical understanding of some of these puzzles [3, 4]. Specifically, for black holes, entropy due to entanglement naturally refers to the measure of the information loss (for an outside observer) due to the spatial separation between the degrees of freedom inside and outside the horizon.

It is well known that the entanglement entropy (EE) or the so-called geometric entropy follows the so-called area law, first demonstrated by Bombelli *et al* [5] and Srednicki [6]. The EE can be derived via many approaches, e.g. in the context of conformal field theories using the so-called replica method [7–11]. This method is also applied to compute the EE for horizons with conical singularities as such [12–14]. In recent years the EE has been found to play crucial roles in understanding many quantum phenomena and their applications [15, 16]. A holographic definition of the EE [17] is proposed as a universal formula to compute entropy of a black hole, in any dimension, using AdS/CFT correspondence, and further attempts are being made to understand its implications [18–20].

Studies on higher-dimensional black holes have become very crucial in order to differentiate the generic features of the black holes with the dimensional specific features. Attempts have been made to investigate thermodynamic properties of higher-dimensional black holes in string the-

ory [21, 22] and loop quantum gravity [23]. In Ref. [24], using the Euclidean path integral approach, it was shown that higher-dimensional (spherically symmetric) rotating black holes obey the Bekenstein-Hawking entropy formula.

Recently, Emparan and Reall obtained an exact solution of a five-dimensional black hole with an event horizon of topology  $S^1 \times S^2$  [25, 26]. These objects can be understood as a circular neutral black string in five dimensions, constructed as the direct product of the Schwarzschild solution and a circle. However, the string has to rotate along  $S^1$  to be stable. The rotating black ring solutions have been rederived in a systematic manner via solution-generating techniques in Refs. [27, 28]. Note that these classes of black holes are not only examples of nonspherical horizon topology but are counterexamples to black hole uniqueness; i.e. the no-hair theorem does not extend to higher dimensions.

Following the work of Emparan and Reall, there have been studies to understand the thermodynamic properties of a black ring. Exact microscopic entropy of non-supersymmetric extremal black rings is exactly reproduced for all values of the ring radius using the same conformal field theory of the four-charge four-dimensional black hole in Ref. [29]. For supersymmetric black rings [30], entropy function was found (from both on-shell and off-shell perspectives) to be reproducing the Bekenstein-Hawking entropy. Further, the higher-order corrections to the entropy arising from the five-dimensional Gauss-Bonnet term and supersymmetric  $R^2$  completion was also computed. In Ref. [31], a string theory description of near-extremal black rings was proposed and the thermodynamic properties were derived for a large family of black rings. Earlier, in Refs. [32, 33] M theory was used to give an exact microscopic accounting of the black ring entropy.

In this work, we compute the EE for scalar field systems propagating with Genus-1 topology to investigate the robustness of the area law. In general we analyze entropy across entangling surfaces with  $S^m \times S^n$  topology. We explicitly compute the EE for  $S^1 \times S^1$  and  $S^1 \times S^2$  horizons.

<sup>‡</sup>Corresponding author

\*email: [santhu@iisertvm.ac.in](mailto:santhu@iisertvm.ac.in)

†email: [suman.ghosh@bose.res.in](mailto:suman.ghosh@bose.res.in)

§email: [shanki@iisertvm.ac.in](mailto:shanki@iisertvm.ac.in)

Although the approaches in Refs. [7–20] provide analytic expressions for the EE, one needs to assume certain symmetries for the underlying theories. However, Genus-1 topology has lesser symmetry than the Genus-0 topologies and hence one cannot use these approaches. In this work, we use *ab initio calculations* or the real-time approach used in Refs. [6, 34, 35] to compute the EE in Genus-1 topologies. The real-time approach has the advantage over the approaches as one can test the robustness of the area law in nonvacuum states [35] and arbitrary dimensions with spherical horizons [36].

As a warmup toward computing EE of massless scalar field propagating in the black rings, in sec. II, we develop the methodology in a 3 + 1- dimensional toroidal coordinate system (i.e. for an entangling surface of topology  $S^1 \times S^1$ ). It is well known that the Helmholtz equation is not separable in toroidal coordinates [37–39]. However, to compute the EE one needs to perform integration over angular dimensions. This can be done in the case of thin rings [40] using perturbative expansion. We use three such approximate methods to simplify our computation and compare the final outcomes for a consistency check. Thereafter, in Sec. III we apply the same technique to compute the EE of black rings ( $S^1 \times S^2$ ). Finally, we end with a brief discussion on the implications of the results obtained and limitations of the methodology developed here.

In this work, we use the  $(+, -, -, -)$  metric signature and set  $\hbar = c = 1$ . Numerical computations are done in MATLAB (R2010b and R2012A) for the lattice size  $N = 100$ , and error in the evaluation of the entanglement entropy is  $10^{-5}$ .

## II. WARM UP: ENTANGLEMENT ENTROPY IN TORUS

### A. Toroidal coordinate system $(r, \phi_1, \phi_2)$

A Toroidal coordinate system in three-dimensional space is well known. For detailed discussion on the coordinate systems, we refer the readers to Refs. [38, 39]. In this subsection, we discuss a few salient features of the coordinate that we use to compute the EE in this geometry.

It is an orthogonal coordinate system that results from rotating the two-dimensional bipolar coordinate system by an angle  $\phi_2$  about the  $Z$  axis [See Fig. (1)]. The two foci are separated by the focal line  $KL$ . The focal line lies in the  $X - Y$  plane and is of length  $2q$ . It passes through the origin  $O$  and makes an angle  $\phi_2$  with  $X$  axis. The location of any point  $P$  in this space is given by  $(r, \phi_1, \phi_2)$ , where

$$r = \ln \left( \frac{PL}{PK} \right), \quad \angle KPL = \phi_1$$

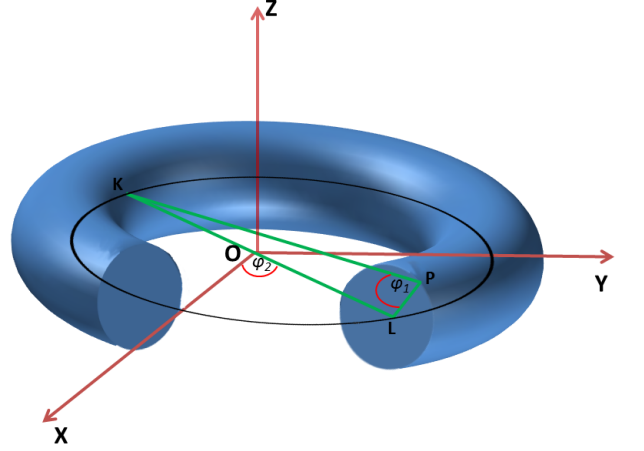


Figure 1: Toroidal coordinate system  $(r, \phi_1, \phi_2)$

The transformation relation between the rectangular  $(X, Y, Z)$  and the toroidal coordinates is given by

$$(X, Y, Z) = \frac{q}{\Delta} (\sinh r \cos \phi_2, \sinh r \sin \phi_2, \sin \phi_1) \quad (1)$$

where,  $\Delta = \cosh r - \cos \phi_1$ . The value range of the coordinates is  $0 \leq r < \infty$ ,  $-\pi \leq \phi_1 \leq \pi$ ,  $0 \leq \phi_2 \leq 2\pi$ .

The torus generated for any surface of constant  $r$  is given by,

$$Z^2 + \left( \sqrt{X^2 + Y^2} - q \coth r \right)^2 = (q \operatorname{csch} r)^2$$

with the center at  $(0, q \coth r)$  in the  $Z - Y$  plane. The outer radius ( $R = q \coth r$ ) and inner radius ( $\rho = q \operatorname{csch} r$ ) of the torus are related to its focal length viz.,  $R^2 - \rho^2 = q^2$  and the metric in this 3 + 1-dimensional space-time is

$$ds^2 = dt^2 - \left( \frac{q}{\Delta} \right)^2 (dr^2 + d\phi_1^2 + \sinh^2 r d\phi_2^2) \quad (2)$$

### B. Approaches to compute entanglement entropy in toroidal geometry

The action for the massless scalar field  $\hat{\Phi}$  propagating in the above background is

$$S = \frac{1}{2} \int dt d^3 \mathbf{r} \sqrt{-g} g^{\mu\nu} \partial_\mu \hat{\Phi} \partial_\nu \hat{\Phi} \quad (3)$$

The form of the action is,

$$S = \frac{1}{2} \int dt d^3 \mathbf{r} \frac{q^3}{\Delta^3} \sinh r \left[ (\partial_t \Phi)^2 - \left( \frac{\Delta}{q} \right)^2 \left[ (\partial_r \Phi)^2 + (\partial_{\phi_1} \Phi)^2 + \frac{1}{\sinh^2 r} (\partial_{\phi_2} \Phi)^2 \right] \right]. \quad (4)$$

As mentioned earlier, the Helmholtz equation is not separable in toroidal coordinates [38, 39]. This implies that the scalar field wave functional cannot be decoupled and the Hamiltonian of the field cannot be written as a product of functionals that depend on only one variable. In the rest of the section we use two approximate — *perturbative* and *constant angle* — approaches to evaluate the EE.

One can use two different schemes for the perturbative approach. The first scheme is to assume that the inner radius is much smaller than the outer radius. In the leading order this scheme leads to an action similar to that of the scalar field in Genus-0 topology. In Appendix A, we discuss this approximation and show that the entropy-area relation is satisfied. The second scheme, which is discussed in the rest of this section, is to consider the limit in which the inner radius ( $\rho$ ) is much smaller than the focal line KL. Unlike the earlier scheme, at all orders of approximation, Genus-1 topology effects will be retained. Under this assumption, we perturbatively expand the action (4) in terms of the inner radius of the torus, in terms of the dimensionless parameter  $x = \rho/q$ .

In the constant angle approach, we fix one of the angles of the Genus-1 topology and evaluate the entropy for the scalar field. The advantage of the constant angle approach compared to the perturbative approach is that the EE can be computed exactly without any approximation. In Appendix B, we show that constant angle approach gives entropy-area relation for all dimensions greater than 2 for Genus-0 topology. We also discuss the importance of this approach. The constant angle  $\phi_1$  approach for the torus geometry leads to sphere of radius  $q/\sin \phi_1$ , centered at  $(0, 0, q \coth \phi_1)$ , and most part of its entangling surface is outside the torus [39, 41]. However, for the black rings, this approach retains Genus-1 topology. We discuss this more in the next section.

### C. Perturbative approach

We use the following ansatz to expand the scalar field in the toroidal geometry (2)

$$\hat{\Phi}(\mathbf{r}, t) = \sum_{\substack{m_1, m_2 \\ = -\infty}}^{\infty} \frac{\hat{\Psi}_{m_1, m_2}(r, t)}{\pi} \cos m_1 \phi_1 \cos m_2 \phi_2 \quad (5)$$

As mentioned earlier, we expand the action in terms of the dimensionless parameter  $x = \rho/q$ . The form of the

action up to the first order in  $x$  is

$$\begin{aligned} S \simeq & \frac{1}{2} \int dt d^3 \mathbf{x} q^3 \left\{ (\partial_t \Psi)^2 - \frac{1}{q^2 x^2} [(\partial_{\Phi_1} \Psi)^2 \right. \\ & \left. + x^3 \left[ \partial_x \left( \frac{\Psi}{\sqrt{x}} \right) \right]^2 + x^2 (\partial_{\Phi_2} \Psi)^2 \right\} \\ & + \frac{1}{2} \int dt d^3 \mathbf{x} q \left[ -\frac{\cos \phi_1 \Psi^2}{x} + 2x \cos \phi_1 (\partial_x \Psi)^2 \right. \\ & \left. + \cos \phi_1 \Psi \partial_x \Psi + \frac{2}{x} \cos \phi_1 (\partial_{\phi_1} \Psi)^2 \right. \\ & \left. - \frac{3}{x} \sin \phi_1 \Psi \partial_{\phi_1} \Psi + 2x \cos \phi_1 (\partial_{\phi_2} \Psi)^2 \right] \quad (6) \end{aligned}$$

where

$$\Psi(\mathbf{x}, t) = \frac{\Phi(\mathbf{x}, t) \sqrt{x}}{(1+x^2)^{1/4} (\sqrt{1+x^2} - x \cos \phi_1)^{3/2}}.$$

Substituting Eq. (5) in Eq. (6) gives

$$\begin{aligned} S = & \frac{1}{2} \sum_{m_1, m_2} \int dt d\rho \left[ \left( \partial_t \tilde{\Psi}_{m_1, m_2} \right)^2 - \left[ \frac{m_1^2}{\rho^2} \tilde{\Psi}_{m_1, m_2}^2 \right. \right. \\ & \left. \left. + \rho \left[ \partial_\rho \left( \frac{\tilde{\Psi}_{m_1, m_2}}{\sqrt{\rho}} \right) \right]^2 + \frac{m_2^2}{q^2} \tilde{\Psi}_{m_1, m_2}^2 \right] \right. \\ & \left. + \frac{2\rho}{q} \left( \partial_\rho \tilde{\Psi}_{m_1, m_2} \right)^2 + \frac{1}{2q} \left( \partial_\rho \tilde{\Psi}_{m_1, m_2}^2 \right) \right. \\ & \left. + \left( \frac{2m_1^2 - 1}{\rho q} + \frac{2\rho m_2^2}{q^3} \right) \tilde{\Psi}_{m_1, m_2}^2 \right] \quad (7) \end{aligned}$$

where  $q\Psi_{m_1, m_2} = \tilde{\Psi}_{m_1, m_2}$  and we assume that  $\Psi_{m_1+1, m_2} = \Psi_{m_1-1, m_2}$ .<sup>1</sup> The Hamiltonian corresponding to the above action is given by

$$\begin{aligned} H = & \frac{1}{2} \sum_{m_1, m_2} \int d\rho \left[ \tilde{\Pi}_{m_1, m_2}^2 - \frac{2\rho}{q} \left( \partial_\rho \tilde{\Psi}_{m_1, m_2} \right)^2 \right. \\ & \left. + \left( \frac{m_1^2}{\rho^2} + \frac{m_2^2}{q^2} + \frac{1 - 2m_1^2}{\rho q} - \frac{2m_2^2 \rho}{q^3} \right) \tilde{\Psi}_{m_1, m_2}^2 \right. \\ & \left. + \rho \left[ \partial_\rho \left( \frac{\tilde{\Psi}_{m_1, m_2}(\rho)}{\sqrt{\rho}} \right) \right]^2 - \frac{\tilde{\Psi}_{m_1, m_2}}{q} \partial_\rho \tilde{\Psi}_{m_1, m_2} \right] \quad (8) \end{aligned}$$

The evaluation of the density matrix requires the discretization of the Hamiltonian. Let  $a$  be the discretization scale and  $\rho = ja, 1 \leq j \leq N$  with constant outer radius, say  $Q$ , such that  $N \ll Q$ . Using the mid-point discretization scheme i.e., the derivative of the form

<sup>1</sup> The approximation is to ensure that the angular modes are independent of each other.

$f(x)d_x[g(x)]$  is replaced by  $f_{j+1/2}[g_{j+1} - g_j]/a$ , the discretized Hamiltonian is given by

$$H = \frac{1}{2a} \sum_{m_1, m_2} \sum_{j=1}^N \left[ \tilde{\Pi}_{m_1 m_2, j}^2 + \left( \frac{m_1^2}{j^2} + \frac{m_2^2}{Q^2} + \frac{1-2m_1^2}{Qj} - \frac{2m_2^2 j}{Q^3} \right) \tilde{\Psi}_{m_1 m_2, j}^2 + \left( j + \frac{1}{2} \right) \left( \frac{\tilde{\Psi}_{m_1 m_2, j+1}}{\sqrt{j+1}} - \frac{\tilde{\Psi}_{m_1 m_2, j}}{\sqrt{j}} \right)^2 - \frac{2(j + \frac{1}{2})}{Q} \left( \tilde{\Psi}_{m_1 m_2, j+1} - \tilde{\Psi}_{m_1 m_2, j} \right)^2 - \frac{\tilde{\Psi}_{m_1 m_2, j}}{Q} \left( \tilde{\Psi}_{m_1 m_2, j+1} - \tilde{\Psi}_{m_1 m_2, j} \right) \right] \quad (9)$$

where  $\tilde{\Psi}_{m_1 m_2, N+1} = 0$ . The commutation relation between the dimensionless field operators is given by

$$[\hat{\tilde{\Psi}}_{m_1 m_2, j}, \hat{\tilde{\Pi}}_{m'_1 m'_2, j'}] = i \delta_{jj'} \delta_{m_1, m'_1} \delta_{m_2, m'_2} \quad (10)$$

The Hamiltonian in Eq. (9) is in the form of a system of  $N$  coupled quantum harmonic oscillators (C1) and can be written as an  $N \times N$  symmetric semidefinite matrix (C2).

Since the Hamiltonian is quadratic (C1), the ground-state wave function can be written as

$$\tilde{\Psi}(x_1, \dots, x_N) = \left( \frac{|\Omega|}{\pi^N} \right)^{1/4} \exp \left[ - \frac{x^T \cdot \Omega \cdot x}{2} \right]. \quad (11)$$

The corresponding density matrix can be evaluated exactly as [6]:

$$\rho(t; t') = \sqrt{\frac{|\Omega|}{\pi^{N-n}|A|}} \exp \left[ - \frac{t^T \gamma t + t'^T \gamma t'}{2} + t^T \beta t' \right], \quad (12)$$

where we have decomposed

$$\Omega \sim K^{1/2} = \begin{pmatrix} A & B \\ B^T & C \end{pmatrix} \quad (13)$$

and defined

$$\beta = \frac{B^T A^{-1} B}{2}; \quad \gamma = C - \beta. \quad (14)$$

$A$  is an  $n' \times n'$  symmetric matrix,  $B$  is an  $n' \times (N - n')$  matrix, and  $C, \beta, \gamma$  are all  $(N - n') \times (N - n')$  symmetric matrices. The matrices  $B$  and  $\beta$  are nonzero only when the Harmonic oscillator (HO)s are interacting.

Performing a series of unitary transformations,

$$V \gamma V^T = \gamma_D = \text{diag}, \quad \bar{\beta} \equiv \gamma_D^{-1/2} V \beta V^T \gamma_D^{-1/2}, \\ W \bar{\beta} W^T = \bar{\beta}_D = \text{diag}, \quad v \equiv W^T \gamma_D^{1/2} V, \quad (15)$$

one can reduce  $\rho(t; t')$  to a product of the reduced density matrices  $\rho_{(2-\text{HO})}(t; t')$  for  $(N - n')$  two coupled HO's with one oscillator traced over (i.e.,  $N = 2, n' = 1$ ) [6],

$$\rho(t; t') = \prod_{i=1}^{N-n} \rho_{(2-\text{HO})}(t; t') \quad (16)$$

$$\rho_{(2-\text{HO})}(t; t') = \sqrt{\frac{|\Omega|}{\pi^{N-n'}|A|}} \exp \left[ - \frac{v_i^2 + v_i'^2}{2} + \bar{\beta}_i v_i v_i' \right]$$

where  $v_i \in v$  and  $\bar{\beta}_i \in \bar{\beta}$ . Correspondingly, the total entanglement entropy is a sum of  $(N - n')$  two-HO entropies  $S_i^{(2-\text{HO})}$  ( $i = 1, \dots, N - n'$ ) which are obtained using the Von Neumann relation

$$S_i^{(2-\text{HO})} = -\ln[1 - \xi_i] - \frac{\xi_i}{1 - \xi_i} \ln \xi_i, \quad \xi_i = \frac{\bar{\beta}_i}{1 + \sqrt{1 - \bar{\beta}_i^2}}. \quad (17)$$

The total entropy for the full Hamiltonian  $H = \sum_{m_1, m_2} H_{m_1 m_2}$ , Eq.(C1), is therefore given by

$$S(n', N) = \sum_{m_1, m_2} S_{m_1 m_2}(n', N) \quad (18)$$

$$S_{m_1, m_2}(n', N) = -\ln[1 - \xi_l] - \frac{\xi_l}{1 - \xi_l} \ln \xi_l. \quad (19)$$

In Fig. 2, we have plotted entanglement entropy vs area

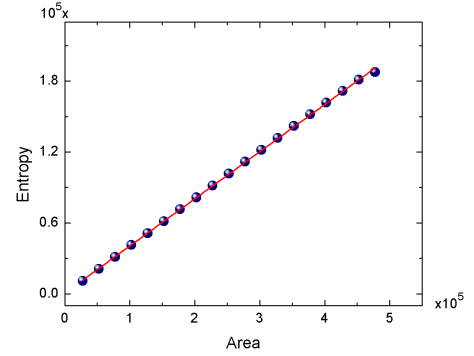


Figure 2: Plot of entropy vs area-relation in the 3+1-dimensional torus using perturbative approach for  $N = 100$ ,  $Q = 5000$ ,  $5 \leq n' \leq 90$ . The blue dots are the numerical outputs and the red line is best linear fit.

of the  $S^1 \times S^1$  surface. As it is clear from the figure, in the linear perturbative limit, the entropy is proportional to area. We will discuss the importance of the result in Sec. IV.

#### D. Constant angle approach

As we mentioned earlier, the constant angle approach for the torus leads to Genus-0 topology and does not provide any information about the higher Genus topology.

However, as discussed in the next section, it does provide useful information in higher dimensions. Below, we discuss the procedure and obtain the EE for by setting  $\phi_1 = \alpha$  for the torus ( $\alpha$  is a constant).

Setting  $\phi_1 = \alpha$  in the action (4), the Hamiltonian corresponding to the reduced action is,

$$H = \frac{1}{2} \sum_m \int d\rho \left[ \tilde{\Pi}_m^2 + \left( \frac{\rho m k_2 \tilde{\Psi}_m}{q^2} \right)^2 + \frac{k_1^2}{q^4} \left[ \partial_\rho \left( k_1 \rho k_2 \tilde{\Psi}_m \right) \right]^2 \right] \quad (20)$$

where,

$$k_1(\rho) = (\rho^2 + q^2)^{1/4} \quad k_2(\rho) = \frac{k_1^2}{\rho} - \cos \alpha$$

$$\tilde{\Psi}_m = \frac{k_2}{q k_1} \Psi_m$$

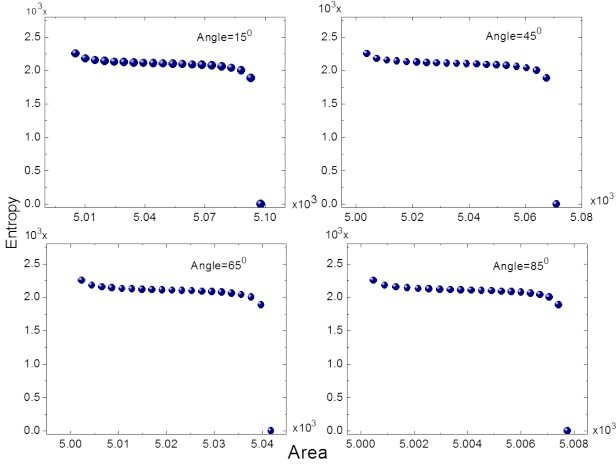


Figure 3: Entropy vs scaled area profile in the 3 + 1 -dimensional torus using *constant angle* approach for  $N = 100$ ,  $Q = 5000$ ,  $5 \leq n' \leq 90$ . The blue dots are the numerical outputs.

As in the previous subsection, to evaluate the EE we need to discretize the Hamiltonian. Here again, the lattice spacing is  $a$  and the outer radius is set to  $Q$ . Using the midpoint discretization scheme, the above Hamiltonian is in the form of a system of  $N$  coupled quantum harmonic oscillators (C1) and can be written as an  $N \times N$  symmetric semidefinite matrix (C3).

Following the procedure discussed in the previous subsection, we obtain the EE for different angles. Fig. 3 shows the profile of the EE vs the larger radius for different constant angles. In the constant angle case, the entangling surface is a cylinder with flat sides and does not vary much with varying  $\rho$  as is clear from Fig. 3; i. e., the domain of the  $x$  axis which is the scaled area of the entangling surface, decreases with increasing  $\phi_1$ , resulting in a constant entropy. As we mentioned earlier, this approach for the torus does not provide insight

on the entropy-area relation, but it helps to confirm our understanding of the nontrivial geometry of constant  $\phi_1$  surfaces.

### III. ENTANGLEMENT ENTROPY IN RING GEOMETRY

Ring geometry is a generalization of the torus for space-times greater than 4. In the case of five-dimensional space-time, the line element corresponding to the ring coordinate ( $S^2 \times S^1$ ) is given in the recent review of Emparan and Reall [26]. In the following subsection, we write down the line element for a general  $S^m \times S^n$ , where  $m, n$  are arbitrary integers with the restriction that both of them simultaneously cannot take the value 1. We then focus on the specific case of evaluating the EE for  $S^2 \times S^1$  using the two approaches discussed in the previous section.

#### A. Ring geometry

Let us consider the  $(m + n + 1)$  -dimensional line-element

$$ds^2 = \sum_{i=1}^m dx_i^2 + \sum_{j=1}^{n+1} dy_j^2 \quad (21)$$

and perform the transformations

$$x_1 = r_1 \cos \phi_1 \quad (22a)$$

$$x_2 = r_1 \sin \phi_1 \cos \phi_2 \quad (22b)$$

$$\vdots$$

$$x_{m-1} = r_1 \sin \phi_1 \sin \phi_2 \dots \cos \phi_{m-1} \quad (22c)$$

$$x_m = r_1 \sin \phi_1 \sin \phi_2 \dots \sin \phi_{m-1} \quad (22d)$$

$$y_1 = r_2 \cos \theta_1 \quad (22e)$$

$$y_2 = r_2 \sin \theta_1 \cos \theta_2 \quad (22f)$$

$$\vdots$$

$$y_n = r_2 \sin \theta_1 \sin \theta_2 \dots \cos \theta_n \quad (22g)$$

$$y_{n+1} = r_2 \sin \theta_1 \sin \theta_2 \dots \sin \theta_n \quad (22h)$$

where  $0 \leq r_1, r_2 < \infty$ ,  $0 \leq \phi_1, \dots, \phi_{m-2}, \theta_1, \dots, \theta_{n-1} \leq \pi$ ,  $0 \leq \phi_{m-1}, \theta_n < 2\pi$ . Substituting the above transformations in Eq. (21), we get

$$ds^2 = dr_1^2 + r_1^2 (d\phi_1^2 + \sin^2 \phi_1 d\phi_2^2 + \dots + \sin^2 \phi_1 \dots \sin^2 \phi_{m-2} d\phi_{m-1}^2) + dr_2^2 + r_2^2 (d\theta_1^2 + \sin^2 \theta_1 d\theta_2^2 + \dots + \sin^2 \theta_1 \dots \sin^2 \theta_{n-1} d\theta_n^2) \quad (23)$$

The above line element corresponds to product to two spaces with the symmetry  $R \times S^\alpha$ , where  $\alpha$  is  $m - 1$  or

$n$ . Performing the transformation

$$r_1 = R \frac{\sin \theta}{\cos \theta + \frac{R}{r}} \quad r_2 = R \frac{\sqrt{\frac{R^2}{r^2} - 1}}{\cos \theta + \frac{R}{r}} \quad (24)$$

to the line element (23), we get [26],

$$ds^2 = \frac{1}{(1 + \frac{r}{R} \cos \theta)^2} \left[ \frac{dr^2}{1 - \frac{r^2}{R^2}} + r^2 (d\theta^2 + \sin^2 \theta d\phi_1^2 + \dots + \sin^2 \theta \sin^2 \phi_1 \dots \sin^2 \phi_{m-2} d\phi_{m-1}^2) \right. \\ \left. + R^2 (1 - \frac{r^2}{R^2}) (d\theta_1^2 + \sin^2 \theta_1 d\theta_2^2 + \dots + \sin^2 \theta_1 \dots \sin^2 \theta_{n-1} d\theta_n^2) \right]. \quad (25)$$

Note that the ranges of  $\theta$  and  $r$  are  $-\pi \leq \theta \leq \pi, 0 \leq r \leq R$ . It is also important to note that  $m$  and  $n$  can take arbitrary values, with the restriction that both of them simultaneously cannot take the value 1. For constant  $R$ , the above line element corresponds to most general Genus-1 topology  $S^m \times S^n$ . The Genus-1 topology is generated by the surfaces of constant  $r$ :

$$x_1^2 + \dots + x_m^2 + \left( \sqrt{y_1^2 + \dots + y_{n+1}^2} - \frac{R^2}{\sqrt{R^2 - r^2}} \right)^2 = \frac{R^2 r^2}{R^2 - r^2} \quad (26)$$

The simplest ring coordinates, as discussed in the review [26], can be obtained by setting  $m = 2$  and  $n = 1$ . For  $m = 2$  and  $n = 1$ , the line element (25) reduces to

$$ds^2 = \frac{1}{(1 + \frac{r}{R} \cos \theta)^2} \left[ \frac{dr^2}{1 - \frac{r^2}{R^2}} + r^2 (d\theta^2 + \sin^2 \theta d\phi_1^2) + R^2 \left( 1 - \frac{r^2}{R^2} \right) d\theta_1^2 \right] \quad (27)$$

It is important to note that the ring geometry is such that the radius ( $r$ ) of the 2-sphere cannot be larger than the radius ( $R$ ) of the circle.

In the case of five -dimensional space, one can embed two different Genus-1 topologies, i. e.,  $S^2 \times S^2$  and  $S^3 \times S^1$ . To embed  $S^3 \times S^1$  topology in six -dimensional space, using the coordinate transformation on to the line element (21),

$$x_1 = r_1 \cos \phi_1 \quad x_2 = r_1 \sin \phi_1 \cos \phi_2 \\ x_3 = r_1 \sin \phi_1 \sin \phi_2 \quad y_1 = r_2 \cos \theta_1 \quad y_2 = r_2 \sin \theta_1 \quad (28)$$

leads to the following line element:

$$ds^2 = \frac{1}{(1 + \frac{r}{R} \cos \theta)^2} \left[ \frac{dr^2}{1 - \frac{r^2}{R^2}} + r^2 (d\theta^2 + \sin^2 \theta d\phi_1^2 + \sin^2 \theta \sin^2 \phi_1 d\phi_2^2) + R^2 (1 - \frac{r^2}{R^2}) d\theta_1^2 \right] \quad (29)$$

where  $r_1$  and  $r_2$  are given by Eqs. (24). Here again the radius ( $r$ ) of the 3-sphere cannot be larger than the radius ( $R$ ) of the circle.

To embed  $S^2 \times S^2$  in six -dimensional space, one starts with same transformation (28); however, changing the definition for  $r_1$  and  $r_2$  in such way that

$$r_1 = R \frac{\sqrt{\frac{R^2}{r^2} - 1}}{\cos \theta + \frac{R}{r}} \quad r_2 = R \frac{\sin \theta}{\cos \theta + \frac{R}{r}} \quad (30)$$

gives

$$ds^2 = \frac{1}{(1 + \frac{r}{R} \cos \theta)^2} \left[ \frac{dr^2}{1 - \frac{r^2}{R^2}} + r^2 (d\theta^2 + \sin^2 \theta d\phi_1^2) + R^2 (1 - \frac{r^2}{R^2}) (d\theta_1^2 + \sin^2 \theta_1 d\theta_2^2) \right] \quad (31)$$

Here again, the radius ( $r$ ) of the 2-sphere cannot be larger than the radius ( $R$ ) of the 2-sphere.

Similarly, we can embed  $S^4 \times S^1$ ,  $S^2 \times S^3$  in seven -dimensional space and  $S^5 \times S^1$ ,  $S^4 \times S^2$ ,  $S^3 \times S^3$  in eight -dimensional space.

## B. Entanglement entropy of scalar fields in black ring

Although the EE can be obtained for a general Genus-1 topology in arbitrary dimensions, we focus on the specific case of black rings in five -dimensional. This is mainly due to two reasons. First, as we go to higher dimensions, it becomes numerically intensive. To compare the computing time to calculate the entanglement entropy for one value for black ring topology and the torus is 60 Peta Flop and 1 Peta Flop, respectively. This increases exponentially as we go to higher dimensions. Second, the torus is a special case of the Genus-1 topology. Comparing the transformations in Secs. II A, III A it is clear that the transformations (22) cannot be used to obtain the torus line element. However, this is not the case for the higher -dimensional generalization of Genus-1 topology.

The action in the  $4+1$  -dimensional ring space-time is

$$S = \frac{1}{2} \int dt d^4 \mathbf{r} \sqrt{g} g^{\mu\nu} \partial_\mu \hat{\Phi} \partial_\nu \hat{\Phi} \quad (32)$$

Using that the ring space-time is a product of  $S^2$  and  $S^1$ , we use the ansatz for the scalar field:

$$\hat{\Phi}(\mathbf{r}, t) = \sum_{l=0}^{\infty} \sum_{m=-l}^l \sum_{n=-\infty}^{\infty} \frac{\chi_{l,m,n}}{\sqrt{\pi}} \mathcal{Z}_{lm}(\theta, \phi_1) \cos n\theta_1 \quad (33)$$

where  $\mathcal{Z}_{lm}$  is the real part of the spherical harmonics.

As in the case of the toroidal background, it is not possible to separate the Helmholtz equation in this background. Hence, it will not be possible to define the ground state of this system exactly. Here again, we use two different — perturbative and constant angle — approaches to compute the entanglement entropy. The two approaches provide complementary information about the entanglement entropy area relation. The perturbative approach will be valid when the radius ( $r$ ) of the 2-sphere is much smaller than the radius ( $R$ ) of the circle. However, the constant angle approach is nonperturbative and one can compute the EE for the case in which  $r \simeq R$ . In the rest of this section, we calculate the EE for the scalar fields using these two approaches.

### C. Perturbative approach

Substituting the ansatz (33) in the action (32), perturbatively expanding the action up to the first order in  $r/R$  and integrating over the angular variables, we get

$$\begin{aligned} S = & \frac{1}{2} \sum_{lmn} \int \tilde{x}^2 R^3 d\eta d\tilde{x} \left[ (\partial_{\eta} \Psi_{lmn})^2 - (\partial_{\tilde{x}} \Psi_{lmn})^2 \right. \\ & \left. + \left( \frac{l(l+1)}{\tilde{x}^2} + n^2 \right) \Psi_{lmn}^2 \right] \\ & - \sum_{l'm'n'} \left( \tilde{x} \partial_{\tilde{x}} \Psi_{lmn} \partial_{\tilde{x}} \Psi_{l'm'n'} I_1 + 2 \Psi_{lmn} \partial_{\tilde{x}} \Psi_{l'm'n'} I_1 \right. \\ & \left. + \frac{1}{\tilde{x}} \Psi_{lmn} \Psi_{l'm'n'} I_2 - \frac{2}{\tilde{x}} \Psi_{lmn} \Psi_{l'm'n'} I_3 \right. \\ & \left. + \frac{1}{\tilde{x}} \Psi_{lmn} \Psi_{l'm'n'} I_4 + n^2 \tilde{x} \Psi_{lmn} \Psi_{l'm'n'} I_1 \right) \quad (34) \end{aligned}$$

where

$$\Psi_{lmn}(\mathbf{x}, t) = \frac{\chi_{lmn}(\mathbf{x}, t)}{(1 + \tilde{x} \cos \phi_1)^2}, \quad (35)$$

$\eta (= t/R)$  and  $\tilde{x} (= r/R)$  are dimensionless variables; and  $I_1, I_2, I_3$  and  $I_4$  are the integrals involving the spherical harmonics given in Eq. (D1). The solutions of these integrals are given in Appendix D.

From the above action it is clear that lowest-order terms gives nonzero values only when  $l = l'$ . This is consistent with the fact the equation corresponding to the lowest-order action satisfies the Sturm-Liouville equation, and, by definition, each of these modes are orthogonal to each other. However, the equation corresponding to the full perturbed action cannot be written in the Sturm-Liouville equation, and, hence it is natural that

first order breaks this. Here, we set  $\Psi_{l+1,m,n} = \Psi_{l-1,m,n}$  which will capture the effect of the first-order term.

Substituting Eq. (D2) in the above action and using the above relation leads to

$$\begin{aligned} S = & \frac{1}{2} \sum_{lmn} \int dt dr \left\{ \left( \partial_t \tilde{\Psi}_{lmn} \right)^2 - r^2 \left[ \partial_r \left( \frac{\tilde{\Psi}_{lmn}}{r} \right) \right]^2 \right. \\ & - \left( \frac{l(l+1)}{r^2} + \frac{n^2}{R^2} + \frac{4C_0 l(l+1)}{rR} + \frac{4C_0 n^2 r}{R^3} \right) \tilde{\Psi}_{lmn}^2 \\ & \left. - \frac{2rC_0}{R} \partial_r \left( \frac{\tilde{\Psi}_{lmn}}{r} \right) \left[ r^2 \partial_r \left( \frac{\tilde{\Psi}_{lmn}}{r} \right) + \tilde{\Psi}_{lmn} \right] \right\} \end{aligned}$$

where

$$\tilde{\Psi}_{lmn} = r \sqrt{R} \Psi_{lmn}, \quad C_0(l, m) = \sqrt{\frac{l^2 - m^2}{4l^2 - 1}} \sim C_1(l, m). \quad (36)$$

Here again, it is important to note that the leading-order terms in the action do not depend on the  $m$  and have the degeneracy factor  $(2l+1)$ ; however, the first-order terms in the action (like  $C_0$ ) have explicit  $m$  dependence. Although this does not have any physical implications, it has implications for the numerical computations. Compared to the torus, here we need to evaluate the entropy for each value of  $m$  and hence the computation time increases exponentially.

The Hamiltonian corresponding to the above action is

$$\begin{aligned} H = & \frac{1}{2} \sum_{lmn} \int dr \left\{ \tilde{\Pi}_{lmn}^2 + r^2 \left[ \partial_r \left( \frac{\tilde{\Psi}_{lmn}}{r} \right) \right]^2 \right. \\ & + \left( \frac{l(l+1)}{r^2} + \frac{n^2}{R^2} + \frac{4C_0 l(l+1)}{rR} + \frac{4C_0 n^2 r}{R^3} \right) \tilde{\Psi}_{lmn}^2 \\ & \left. + \frac{2rC_0}{R} \partial_r \left( \frac{\tilde{\Psi}_{lmn}}{r} \right) \left[ r^2 \partial_r \left( \frac{\tilde{\Psi}_{lmn}}{r} \right) + \tilde{\Psi}_{lmn} \right] \right\} \quad (37) \end{aligned}$$

where  $\hat{\Pi}_{lmn}(r)$  is canonically conjugate to  $\hat{\Psi}_{lmn}(r)$ , and it satisfies

$$[\hat{\Psi}_{lmn}(r), \hat{\Pi}_{l'm'n'}(r')] = i\delta(r-r')\delta_{l,l'}\delta_{m,m'}\delta_{n,n'} \quad (38)$$

As in the earlier calculations, to evaluate the EE we need to discretize the Hamiltonian. Here again the lattice spacing is  $a$  and  $R = aQ$ . Using the midpoint discretization scheme, the above Hamiltonian is in the form of a system of  $N$  coupled quantum harmonic oscillators C1 and can be written as a  $N \times N$  symmetric semidefinite matrix (C4).

The total entropy for the full Hamiltonian  $H = \sum_{l,m_1,m_2} H_{lm_1 m_2}$ , is given by

$$S(n', N) = \sum_{l,m,n} S_{lmn}(n', N) \quad (39)$$

$$S_{lmn}(n', N) = -\ln[1 - \xi_i] - \frac{\xi_i}{1 - \xi_i} \ln \xi_i. \quad (40)$$

where  $\xi_i$  are given by Eq. (17).

In Fig. 4, we have plotted the EE vs area of the  $S^2 \times S^1$  surface. As it is clear from the figure, in the linear perturbative limit, the entropy is proportional to area. We will discuss the importance of the result in Sec. IV.

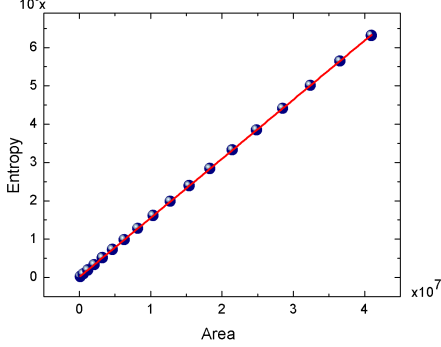


Figure 4: Entropy versus scaled area profile in the 4 + 1 D black rings using *perturbative* approach for  $N = 100$ ,  $Q = 5000$ ,  $5 \leq n' \leq 90$ . The blue dots are the numerical outputs and the red line is best linear fit.

#### D. Constant angle approach

By setting the angle  $\phi_1$  to a constant ( $\alpha$ ), the action (32) reduces to

$$S = \frac{1}{2} \sum_{m_1, m_2} \int dt dr \left[ \left( \partial_t \tilde{\Psi}_{m_1, m_2} \right)^2 - \left( 1 + \frac{r}{R} \cos \alpha \right)^2 \times \left[ r \left( 1 - \frac{r^2}{R^2} \right) \left( \partial_r \left( \frac{\tilde{\Psi}_{m_1, m_2}}{\sqrt{r}} \right) + \frac{3 \cos \alpha}{2R} \tilde{\Psi}_{m_1, m_2} \right)^2 + \left( \frac{m_1^2}{r^2 \sin^2 \alpha} + \frac{m_2^2}{R^2 - r^2} \right) \tilde{\Psi}_{m_1, m_2}^2 \right] \right] \quad (41)$$

where

$$\tilde{\Psi}_{m_1, m_2} = \sqrt{\frac{Rr \sin \alpha}{\left( 1 + \frac{r}{R} \cos \alpha \right)}} \Phi_{m_1, m_2}$$

The Hamiltonian corresponding to the above reduced action is:

$$H = \frac{1}{2} \sum_{m_1, m_2} \int dr \left[ \tilde{\Pi}_{m_1, m_2}^2 + \left( 1 + \frac{r}{R} \cos \alpha \right)^2 \left[ r \left( 1 - \frac{r^2}{R^2} \right) \left( \partial_r \left( \frac{\tilde{\Psi}_{m_1, m_2}}{\sqrt{r}} \right) + \frac{3 \cos \alpha}{2R} \tilde{\Psi}_{m_1, m_2} \right)^2 + \left( \frac{m_1^2}{r^2 \sin^2 \alpha} + \frac{m_2^2}{R^2 - r^2} \right) \tilde{\Psi}_{m_1, m_2}^2 \right] \right] \quad (42)$$

where  $\tilde{\Pi}_{m_1, m_2}$  is canonically conjugate to  $\tilde{\Psi}_{m_1, m_2}$  and

$$\tilde{\Psi}_{m_1, m_2} = \sqrt{\frac{Rr \sin \alpha}{\left( 1 + \frac{r}{R} \cos \alpha \right)}} \Psi_{m_1, m_2}$$

Discretizing the Hamiltonian and following the procedure discussed above, we obtain the entropy for different angles. Fig. 5 shows the plot of entropy vs the area for different angles. The plots show that the entanglement entropy is linearly related to area.

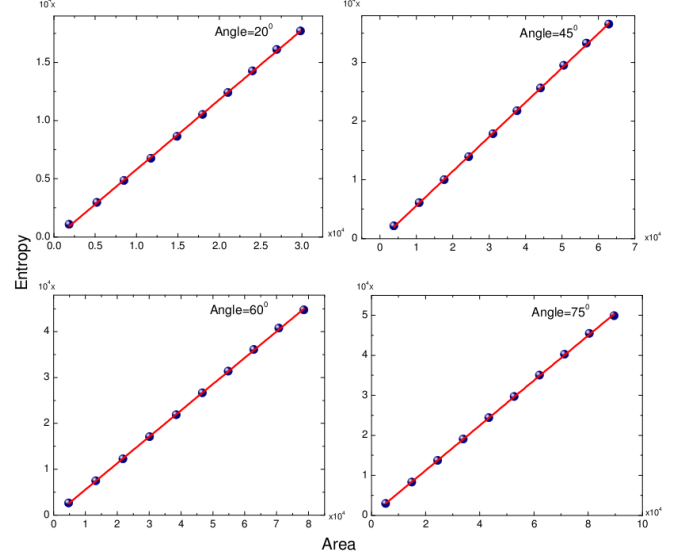


Figure 5: Entropy versus scaled area profile in the 4 + 1 D black rings using *constant angle* approach for  $N = 100$ ,  $Q = 5000$ ,  $5 \leq n' \leq 90$ . The blue dots are the numerical outputs and the red line is best linear fit.

#### IV. CONCLUSIONS AND DISCUSSIONS

In this work, we have obtained the entanglement entropy of massless, minimally coupled scalar fields in Genus-1 topologies. Specifically, we have shown that the entanglement entropy is linearly related to the area of the torus ( $S^1 \times S^1$ ) and ring geometry ( $S^2 \times S^1$ ).

Genus-1 topologies have lesser symmetry compared to Genus-0 topologies, and hence we use *ab-initio* calculations to obtain entanglement entropy in these topologies. One of the main difficulties in evaluating entanglement entropy in Genus-1 topologies is that the Helmholtz equation is not separable. This implies that the one will not be able to write down the ground-state wave function exactly. To circumvent this problem, we have used two complementary approaches to evaluate entanglement entropy. In the first approach we have assumed that the ratio of the smaller radius to the larger radius is much less than unity. In the second approach, we evaluated the entanglement entropy by setting one of the angular



coordinates to be constant. In this case, the entanglement entropy can be evaluated exactly as the effective Helmholtz equation is separable.

Both these approaches clearly show that the entanglement entropy is proportional to the area of the Genus-1 constant radius surface. In several ways, the result cannot be extrapolated from the case of the sphere. First, the Genus-1 topologies are not simply connected like the spheres. Second, it has been shown that most of the contribution to the entanglement entropy comes from close to the surface [3]. In the case of Genus-1, since the surface is not simply connected, it is not obvious that only the short-range effects will dominate. Our analysis in this work, shows that this is indeed the case.

The result brings attention to the following interesting questions. Does the presence of mass to the scalar field affect the entanglement entropy relation for Genus-1 topologies? Does the entanglement entropy-area law hold for Genus-2 or higher surfaces? In Appendix B we show that the constant angle approach for the spherical geometry fixes the proportionality constant. It will be interesting to know whether one can use this approach to analytically obtain entanglement entropy in higher dimensions with the subleading corrections.

We hope to return to study these problems in the near future.

### Acknowledgments

The work is supported by Max Planck-India Partner Group on Gravity and Cosmology. S.S.K acknowledges CSIR, Government. of India, for the financial support. S.G acknowledges the hospitality at IISER-TVM, where the initial part of this work was done. S.S is partially supported by Ramanujan Fellowship of DST, India. Part of the numerical computations were performed on the supercomputing clusters at Albert Einstein Institute, Golm.

### Appendix A: Thin inner radii ( $r/R \ll 1$ ) approximation for Torus

In this appendix, we calculate the entanglement entropy for a thin torus, i. e.,  $r \gg 1$ , such that

$$\Delta \sim \cosh r \sim \sinh r \quad (\text{A1})$$

This approximation (A1) implies that  $r$  takes a minimum value, say  $\beta$ , which is always positive. Substituting Eq.(5) in Eq. (4) with this approximation, we get

$$S \sim \frac{1}{2} \sum_{m_1, m_2} \int dt \int_{\beta}^{\infty} q dr \left[ \frac{q^2}{\Delta^2} (\partial_t \Psi_{m_1, m_2})^2 - (\partial_r \Psi_{m_1, m_2})^2 - \left( m_1^2 + \frac{m_2^2}{\sinh^2 r} \right) \Psi_{m_1, m_2}^2 \right] \quad (\text{A2})$$

Rewriting Eq.(A2) in terms of inner radius of the torus, we get

$$S = \frac{1}{2} \sum_{m_1, m_2} \int dt \int_0^{\infty} d\rho \left[ \left( \partial_t \tilde{\Psi}_{m_1, m_2} \right)^2 - \rho \left[ \partial_{\rho} \left( \frac{\tilde{\Psi}_{m_1, m_2}}{\sqrt{\rho}} \right) \right]^2 - \left( \frac{m_1^2}{\rho^2} + \frac{m_2^2}{q^2} \right) \tilde{\Psi}_{m_1, m_2}^2 \right] \quad (\text{A3})$$

where  $\sqrt{q\rho} \Psi_{m_1, m_2} = \tilde{\Psi}_{m_1, m_2}$ . The corresponding Hamiltonian is

$$H = \frac{1}{2} \sum_{m_1, m_2} \int_0^{\infty} d\rho \left[ \tilde{\Pi}_{m_1, m_2}^2 + \rho \left[ \partial_{\rho} \left( \frac{\tilde{\Psi}_{m_1, m_2}}{\sqrt{\rho}} \right) \right]^2 + \left( \frac{m_1^2}{\rho^2} + \frac{m_2^2}{q^2} \right) \tilde{\Psi}_{m_1, m_2}^2 \right] \quad (\text{A4})$$

The discretized Hamiltonian is

$$H = \frac{1}{2a} \sum_{m_1, m_2} \sum_{j=1}^N \left[ \tilde{\Pi}_{m_1 m_2, j}^2 + \left( \frac{m_1^2}{j^2} + \frac{m_2^2}{Q^2} \right) \tilde{\Psi}_{m_1 m_2, j}^2 + \left( j + \frac{1}{2} \right) \left( \frac{\tilde{\Psi}_{m_1 m_2, j+1}}{\sqrt{j+1}} - \frac{\tilde{\Psi}_{m_1 m_2, j}}{\sqrt{j}} \right)^2 \right] \quad (\text{A5})$$

In Fig. 6 we have plotted EE by following the procedure discussed in Sec. II. It is clear from the plot that the entropy-area relation is satisfied in this limit.

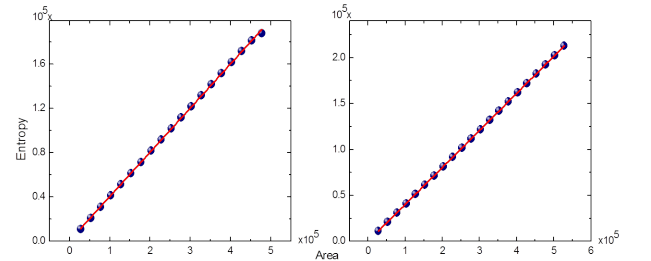


Figure 6: Entropy versus scaled area profile in the 3 + 1 D torus having thin inner radii with  $N = 100(200)$ ,  $Q = 5000$ ,  $5 \leq n' \leq 95$  ( $5 \leq n' \leq 195$ ) respectively. The blue dots are the numerical outputs and the red line is best linear fit.

### Appendix B: Constant angle- Spherical case

In this work, we have used the constant angle approach to obtain the entanglement entropy for a Genus-1 surface. The approach is necessitated by the fact that in nonzero Genus topologies the Helmholtz equation is not separable.

Applying this approach in the spherical case leads to an interesting result. One of the criticisms of entanglement entropy is the that the prefactor of the entanglement entropy-area relation is undetermined [2]. In this appendix we show that the constant angle approach may provide a plausible way of fixing the coefficient in the entropy-area relation and that the approach may provide subleading corrections to the area law.

Recently, one of the authors along with Das and Braunstein [36] have shown that the entanglement entropy-area law is valid for  $D$ -Sphere  $D > 1$ . To understand the importance of the constant angle approach, let us set the polar angle ( $\theta = \alpha$ ) to be a constant value in the 3-Sphere ( $r, \theta, \phi_1, \phi_2$ ). The reduced line element is,

$$ds^2 = dt^2 - [dr^2 + r^2 \sin^2 \alpha (d\phi_1^2 + \sin^2 \phi_1 d\phi_2^2)] \quad (B1)$$

The above equation is similar to an effective line element in the  $3 + 1$  -dimensional for which the Hamiltonian is

$$H = \frac{1}{2} \sum_{l,m} \int dr \left[ \tilde{\Pi}_{lm}^2 + r^2 \left[ \partial_r \left( \frac{\tilde{\Psi}_{lm}}{r} \right) \right]^2 + \frac{l(l+1)}{r^2 \sin^2 \alpha} \tilde{\Psi}_{lm}^2 \right] \quad (B2)$$

where we have used the following ansatz for expanding the action

$$\Phi(t, r, \phi_1, \phi_2) = \sum_{l,m} \frac{\tilde{\Psi}_{lm}(t, r)}{r \sin \alpha} \mathcal{Z}_{l,m}(\phi_1, \phi_2).$$

From the Fig. 7, it is interesting to note that the EE varies linearly with the angle-dependent area (proportional to  $\sin^2 \alpha$ ), which is identical to the case of the three -dimensional sphere [6] with the slope being 0.29.

In the same way, one can start with the line element in the  $(3 + 1)$  -dimensional space-time  $(t, r, \theta, \phi)$  and set the polar angle to be a constant leading to an effective line element in the  $(2 + 1)$  -dimensional space-time

$$ds^2 = dt^2 - [dr^2 + r^2 \sin^2 \alpha d\phi^2] \quad (B3)$$

The form of the effective two -dimensional Hamiltonian is,

$$H = \frac{1}{2} \sum_m \int dr \left[ \tilde{\Pi}_m^2 + r \left[ \partial_r \left( \frac{\tilde{\Psi}_m}{\sqrt{r}} \right) \right]^2 + \frac{m^2}{r^2 \sin^2 \alpha} \tilde{\Psi}_m^2 \right] \quad (B4)$$

Again the ansatz has the form,

$$\Phi(t, r, \phi) = \sum_{m=-\infty}^{\infty} \frac{\tilde{\Psi}_m(t, r)}{\sqrt{\pi r \sin \alpha}} \cos m\phi$$

Repeating the same procedure as discussed earlier, the plot of the EE as a function of area showing that the entropy is proportional to  $\sin \alpha$  is shown in Fig8.

In the same way, the entanglement entropy for the scalar fields in the reduced  $(2 + 1)$  -dimensional space-time leads to the relation

$$S_{ent}^{(1+1)} = k_0 \ln(r/a) \quad (B5)$$

where  $a$  is the lattice spacing and  $k_0$  is a constant [9]. Unlike the higher-dimensional space-times, in this case

the constant angle entanglement entropy is *independent* of the angle. This provides an interesting possibility of obtaining the higher -dimensional entanglement entropy from the above logarithmic dependence (B5). Specifically, it is interesting to note that the entanglement entropy for the scalar field in  $(2+1)$ -dimensional space-time can be obtained by integrating Eq. (B5) with respect to  $\alpha$ , i. e.,

$$\begin{aligned} S_{ent}^{(2+1)} &= \int_{\alpha=0}^{\alpha=2\pi} r d\alpha k_0 \ln(r/a) \\ &= 2\pi r k_0 \ln(1/a) + 2\pi r k_0 \ln r \\ &= 2\pi r k_1 + 2\pi r k_0 \ln r \end{aligned} \quad (B6)$$

where  $k_1 = k_0 \ln(1/a)$ . Note that  $a \ll 1$ ; hence  $k_1 > 0$ . A similar procedure can be applied to obtain the EE for  $3 + 1$  dimensions:

$$S_{ent}^{(3+1)} = 4\pi r^2 k_1 + k_0 r^2 \int_{\alpha=0}^{\alpha=\pi} d\alpha \sin \alpha \ln(r^2 \sin \alpha) \quad (B7)$$

Thus, by fixing the constant  $k_0$  we can calculate the corrections to the EE for  $(D + 1)$ -sphere symmetric space-time as

$$S_{ent}^{(D+1)} = 4\pi r^{D-1} k_1 + f(k_0) \quad (B8)$$

where  $f(k_0)$  is the correction to the  $D + 1$  -dimensional entropy, which is a function of  $k_0$  only. It interesting to note that the area- dependent terms only depend on  $k_1$  and are determined. we have yet to understand the full implications of the above result and it is currently being investigated.

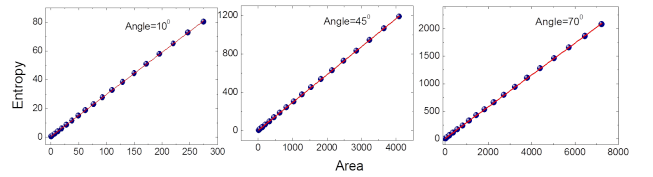


Figure 7: Entropy versus reduced area for constant angle approach in the case of effective 3-D space with the number of sites is  $N=100$  ( $5 \leq n' \leq 95$ ). The blue dots are the numerical outputs and the red line is best linear fit.

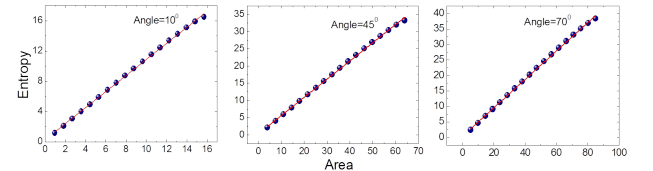


Figure 8: Entropy versus the reduced area for constant angle in the case of effective 2-D space with the number of sites is  $N=100$  ( $5 \leq n' \leq 95$ ). The blue dots are the numerical outputs and the red line is best linear fit.

### Appendix C: Matrix elements in toroidal and ring geometries

The interaction matrix that is used for computing the EE in all different methods is given. The Hamiltonian of the system can be written as,

$$H = \frac{1}{2} \sum_{i=1}^N \Pi^2(x) + \frac{1}{2} \sum_{i,j=1}^N x_i K_{ij} x_j \quad (C1)$$

where  $K_{ij}$  is the interaction matrix elements.

- *Perturbative approach in toroidal co-ordinates*

$$K_{ij} = \left[ \frac{3}{2} - \frac{1}{Q} + \left( m_1^2 + \frac{m_2^2}{Q^2} \right) \left( 1 - \frac{2}{Q} \right) \right] \delta_{i1} \delta_{j1} + \left[ 2 + \frac{1}{Q} \left( 1 - 4j + \frac{1}{j} \right) + m_1^2 \left( \frac{1}{j^2} - \frac{2}{Qj} \right) + \frac{m_2^2}{Q^2} \left( 1 - \frac{2j}{Q} \right) \right] \delta_{ij} \\ + \left[ \frac{2(j + \frac{1}{2})}{Q} - \frac{1}{2Q} - \frac{j + \frac{1}{2}}{\sqrt{j(j+1)}} \right] \delta_{ij+1} + \left[ \frac{2(i + \frac{1}{2})}{Q} - \frac{1}{2Q} - \frac{i + \frac{1}{2}}{\sqrt{i(i+1)}} \right] \delta_{ij-1} \quad (C2)$$

- *Constant angle approach in toroidal co-ordinates*

$$K_{ij} = \left[ \frac{\left( \sqrt{1+Q^2} - \cos \alpha \right)^2}{Q^4} \left( \sqrt{\left( \frac{9}{4} + Q^2 \right) (1+Q^2) + m^2} \right) \right] \delta_{i1} \delta_{j1} + \left[ \frac{\left( \sqrt{1 + \left( \frac{Q}{j} \right)^2} - \cos \alpha \right)^2}{Q^4} j^2 \sqrt{j^2 + Q^2} \right. \\ \times \left( \sqrt{\left( j - \frac{1}{2} \right)^2 + Q^2} + \sqrt{\left( j + \frac{1}{2} \right)^2 + Q^2} + \frac{m^2}{\sqrt{j^2 + Q^2}} \right) \left. \right] \delta_{ij} - \left[ \frac{\sqrt{\left( j + \frac{1}{2} \right)^2 + Q^2}}{Q^4} \right. \\ \times j(j+1) \left( ((j+1)^2 + Q^2)(j^2 + Q^2) \right)^{1/4} \left( \sqrt{1 + \left( \frac{Q}{j} \right)^2} - \cos \alpha \right) \left( \sqrt{1 + \left( \frac{Q}{j+1} \right)^2} - \cos \alpha \right) \left. \right] \delta_{ij+1} \\ - \left[ \frac{\sqrt{\left( i + \frac{1}{2} \right)^2 + Q^2}}{Q^4} i(i+1) \left( ((i+1)^2 + Q^2)(i^2 + Q^2) \right)^{1/4} \left( \sqrt{1 + \left( \frac{Q}{i} \right)^2} - \cos \alpha \right) \right. \\ \times \left( \sqrt{1 + \left( \frac{Q}{i+1} \right)^2} - \cos \alpha \right) \left. \right] \delta_{ij-1} \quad (C3)$$

- *Perturbative approach in ring co-ordinates*

$$K_{ij} = \left[ \frac{9}{4} + l(l+1) + \frac{n^2}{Q^2} + C_0 \left( \frac{4n^2}{Q^3} + \frac{4l(l+1)}{Q} - \frac{21}{4Q} \right) \right] \delta_{i1} \delta_{j1} + \left[ 2 + \frac{1}{2j^2} + \frac{l(l+1)}{j^2} + \frac{n^2}{Q^2} \right. \\ + C_0 \left( \frac{4j}{Q} + \frac{3}{Qj} - 8 \frac{j + \frac{1}{2}}{jQ} + 4 \frac{n^2 j}{Q^3} + 4 \frac{l(l+1)}{jQ} \right) \left. \right] \delta_{ij} + \left[ - \frac{\left( j + \frac{1}{2} \right)^2}{j(j+1)} + \frac{2C_0 \left( j + \frac{1}{2} \right)}{Q(j+1)} \left( 2 - \frac{\left( j + \frac{1}{2} \right)^2}{j} \right) \right] \delta_{ij+1} \\ + \left[ - \frac{\left( i + \frac{1}{2} \right)^2}{i(i+1)} + \frac{2C_0 \left( i + \frac{1}{2} \right)}{Q(i+1)} \left( 2 - \frac{\left( i + \frac{1}{2} \right)^2}{i} \right) \right] \delta_{ij-1} \quad (C4)$$

• *Constant angle approach in ring co-ordinates*

$$\begin{aligned}
K_{ij} &= \left[ \frac{\frac{3}{2} \left(1 - \frac{9}{4Q^2}\right)}{1 + \frac{3}{2Q} \cos \alpha} \left(1 + \frac{\cos \alpha}{Q}\right)^3 + \left(\frac{m_1^2}{\sin^2 \alpha} + \frac{m_2^2}{Q^2 - 1}\right) \left(1 + \frac{\cos \alpha}{Q}\right)^2 \right] \delta_{i1} \delta_{j1} + \left(1 + \frac{j \cos \alpha}{Q}\right)^3 \\
&\times \left[ \frac{(j - \frac{1}{2}) \left(1 - \frac{(j - \frac{1}{2})^2}{Q^2}\right)}{j \left(1 + \frac{(j - \frac{1}{2}) \cos \alpha}{Q}\right)} + \frac{(j + \frac{1}{2}) \left(1 - \frac{(j + \frac{1}{2})^2}{Q^2}\right)}{j \left(1 + \frac{(j + \frac{1}{2}) \cos \alpha}{Q}\right)} + \left(\frac{m_1^2}{j^2 \sin^2 \alpha} + \frac{m_2^2}{Q^2 - j^2}\right) \left(1 + \frac{j \cos \alpha}{Q}\right)^{-1} \right] \delta_{ij} \\
&- \left[ \frac{(j + \frac{1}{2}) \left(1 - \frac{(j + \frac{1}{2})^2}{Q^2}\right)}{\left(1 + \frac{(j + \frac{1}{2}) \cos \alpha}{Q}\right)} \frac{\left(1 + \frac{j \cos \alpha}{Q}\right)^{\frac{3}{2}}}{\sqrt{j(j+1)}} \left(1 + \frac{(j+1) \cos \alpha}{Q}\right)^{\frac{3}{2}} \right] \delta_{ij+1} \\
&- \left[ \frac{(i + \frac{1}{2}) \left(1 - \frac{(i + \frac{1}{2})^2}{Q^2}\right)}{\left(1 + \frac{(i + \frac{1}{2}) \cos \alpha}{Q}\right)} \frac{\left(1 + \frac{i \cos \alpha}{Q}\right)^{\frac{3}{2}}}{\sqrt{i(i+1)}} \left(1 + \frac{(i+1) \cos \alpha}{Q}\right)^{\frac{3}{2}} \right] \delta_{ij-1} \quad (C5)
\end{aligned}$$

#### Appendix D: Evaluation of integrals

The integrals in Eq.(32) are listed below and can be evaluated exactly [41, 42]:

$$I_1 = \int_0^\pi \int_0^{2\pi} \mathcal{Z}_{lm} \cos \theta \mathcal{Z}_{l'm'} d\Omega \quad (D1a)$$

$$I_2 = \int_0^\pi \int_0^{2\pi} \partial_\theta \mathcal{Z}_{lm} \cos \theta \partial_\theta \mathcal{Z}_{l'm'} d\Omega \quad (D1b)$$

$$I_3 = \int_0^\pi \int_0^{2\pi} \mathcal{Z}_{lm} \sin \theta \partial_\theta \mathcal{Z}_{l'm'} d\Omega \quad (D1c)$$

$$I_4 = \int_0^\pi \int_0^{2\pi} \partial_{\phi_1} \mathcal{Z}_{lm} \frac{\cos \theta}{\sin^2 \theta} \partial_{\phi_1} \mathcal{Z}_{l'm'} d\Omega \quad (D1d)$$

$$I_1 = [C_0 \delta_{l',l-1} + C_1 \delta_{l',l+1}] \delta_{m,m'} \quad (D2a)$$

$$I_3 = [-(l+1)C_0 \delta_{l',l-1} + lC_1 \delta_{l',l+1}] \delta_{m,m'} \quad (D2b)$$

$$I_4 = \frac{m}{2} [(2l-1)C_0 \delta_{l',l-1} + (2l+3)C_1 \delta_{l',l+1}] \delta_{m,m'} \quad (D2c)$$

$$I_2 = l(l+1)I_1 + I_3 - I_4 \quad (D2d)$$

where,  $d\Omega = \sin \theta d\theta d\phi_1$  and

$$C_0 = \sqrt{\frac{l^2 - m^2}{4l^2 - 1}}, \quad C_1 = \sqrt{\frac{(l-m+1)(l-m+1)}{(2l+1)(2l+3)}}.$$

- [1] J. M. Bardeen, B. Carter, and S. W. Hawking, Commun. Math. Phys. **31**, 161 (1973);  
J. D. Bekenstein, Lett. Nuovo Cimento **4**, 737 (1972);  
G. 't Hooft, Nucl. Phys. **B256**, 727 (1985);  
J. D. Bekenstein, Contemp. Phys. **45**, 31 (2004);  
D. N. Page, New J.Phys. **7**, 203 (2005).
- [2] Robert M. Wald, Living Rev. Relativity **4**, 66 (2001).
- [3] Saurya Das, S. Shankaranarayanan, and Sourav Sur, Horizons in World Physics, edited by M. Everett and L. Pedroza, **268**, 211 Nova Science Publisheres (2009).
- [4] Sergey N. Solodukhin, Living Rev. Relativity **14**, 8 (2011).
- [5] L. Bombelli, R. K. Koul, J.-H. Lee, and R. D. Sorkin,

- Phys. Rev.D **34**, 373 (1986).
- [6] M. Srednicki, Phys. Rev. Lett. **71**, 666 (1993).
- [7] C. Holzhey, F. Larsen, and F. Wilczek, Nucl. Phys. **B424**, 443 (1994)
- [8] C. Callan and F. Wilczek, Phys. Lett. B **333**, 55 (1994).
- [9] P. Calabrese and J. Cardy, J.Stat. Mech. , P06002 (2004) ; Int.J.Quant.Inf. **4** 429 (2006).
- [10] G. Vidal, J. I. Latorre, E. Rico, and A. Kitaev, Phys. Rev. Lett. **90**, 227902 (2003).
- [11] J. I. Latorre, E. Rico, and G. Vidal, Quant. Inf. and Comp. **4**, 048 (2004).
- [12] S. N. Solodukhin, Living Rev. Relativity **14**, (2011) ;  
S. N. Solodukhin, Phys. Rev. D **51**, 618 (1995) ;

- S. N. Solodukhin, Phys. Rev. D **51**, 609 (1995) ;  
 R. B. Mann and S. N. Solodukhin, Nucl. Phys. **B523**, 293 (1998).
- [13] H. Casini and M. Huerta, Nucl. Phys. **B764**, 183, (2007).  
 [14] H. Casini and M. Huerta, Phys. Lett. B **694**, 167 (2010).  
 [15] R. Horodecki, P. Horodecki, M. Horodecki, and K. Horodecki, Rev. Mod. Phys. **81**, 865 (2009).  
 [16] J. Eisert, M. Cramer, and M. B. Plenio, Rev. Mod. Phys. **82**, 277 (2010).  
 [17] S. Ryu and T. Takayanagi, Phys. Rev. Lett. **96**, 181602 (2006).  
 [18] S. Ryu and T. Takayanagi, JHEP **0608**, 045 (2006).  
 [19] H. Casini, M. Huerta, and R. C. Myers, JHEP **1105**, 036 (2011).  
 [20] A. Lewkowycz and J. Maldacena, JHEP **08**, 090 (2013).  
 [21] M. Cvetič and D. Youm, Nucl. Phys. **B477**, 449 (1996).  
 [22] A. Chamblin, R. Emparan, C. V. Johnson, and R. C. Myers, Phys. Rev. D **60**, 064018 (1999).  
 [23] N. Bodendorfer, Phys. Lett. B **726**, 887 (2013).  
 [24] Z. Z. Ma, Prog. Theor. Phys. **115**, 863 (2006).  
 [25] R. Emparan and H. S. Reall, Phys. Rev. Lett. **88**, 101101 (2002).  
 [26] R. Emparan and H. S. Reall, Class. Quant. Grav. **23**, R169, (2006).  
 [27] H. Iguchi and T. Mishima, Phys. Rev. D **73**, 121501 (2006).
- [28] S. S. Yazadjiev, Phys. Rev. D **73**, 104007 (2006).  
 [29] R. Emparan, Class. Quant. Grav. **25**, 175005 (2008).  
 [30] R.-G. Cai and D.-W. Pang, JHEP **0704**, 027 (2007).  
 [31] F. Larsen, JHEP **0510**, 100 (2005).  
 [32] M. Cyrier, M. Guica, D. Mateos, and A. Strominger, Phys. Rev. Lett. **94**, 191601 (2005).  
 [33] S. Datta and J. R. David, arXiv:hep-th/1311.1218.  
 [34] M. B. Plenio, J. Eisert, J. Dreissig, and M. Cramer, Phys. Rev. Lett. **94**, 060503 (2005).  
 [35] S. Das, S. Shankaranarayanan, and S. Sur, Phys. Rev. D **77**, 064013 (2008).  
 [36] S. L. Braunstein, S. Das, and S. Shankaranarayanan, JHEP **07**, 130 (2013).  
 [37] M. S. Janaki and B. Dasgupta, IEEE Trans. Plasma Sci., **18**, 78 (1990).  
 [38] P. M. Morse and H. Feshbach, *Methods of Theoretical Physics (I)*, McGraw-Hill, New York (1953).  
 [39] P. Moon and D. E. Spencer, *Field Theory Handbook: Including Coordinate Systems, Differential Equations and Their Solutions*, 2nd ed., Springer, New York (1971).  
 [40] J. Kunz, arXiv:gr-qc/1309.4049.  
 [41] G. B. Arfken and H. J. Weber, *Mathematical Methods for Physicists*, (6th ed.), pp 804, Elsevier Academic Press (2004).  
 [42] M. A. Rashid, J. Phys. A: Math. Gen. **19**, 2505 (1986).